

Time-Domain Finite Elements for Virtual Testing of Electromagnetic Compatibility

Vladimír ŠEDĚNKA¹, Jan CIGÁNEK¹, Petr KADLEC¹, Zbyněk RAIDA¹,
Michal WIKTOR², Maria Sabrina SARTO³, Sandra GRECO³

¹ Dept. of Radio Electronics, Brno University of Technology, Purkyňova 118, 612 00 Brno, Czech Republic

² Dept. of Informatics and Statistics, Medical University of Gdansk, Curie Skłodowskiej 3a, 80-952 Gdańsk, Poland

³ Dept. of Astronautical, Electrical and Energy Engineering, Sapienza Univ. of Rome, P.le A. Moro 5, 00185 Rome, Italy

xseden01@stud.feec.vutbr.cz, xcigan02@stud.feec.vutbr.cz, xkadle19@stud.feec.vutbr.cz, raida@feec.vutbr.cz,
wiktor.michal@gmail.com, mariasabrina.sarto@uniroma1.it, sandra.greco@uniroma1.it

Abstract. *The paper presents a time-domain finite-element solver developed for simulations related to solving electromagnetic compatibility issues. The software is applied as a module integrated into a computational framework developed within a FP7 European project High Intensity Radiated Field – Synthetic Environment (HIRF SE) able to simulate a large class of problems. In the paper, the mathematical formulation is briefly presented, and special emphasis is put on the user point of view on the simulation tool-chain. The functionality is demonstrated on the computation of shielding effectiveness of two composite materials. Results are validated through experimental measurements and agreement is confirmed by automatic feature selective algorithms.*

Keywords

Amelet-HDF, electromagnetic compatibility (EMC), high intensity radiated field synthetic environment (HIRF SE), shielding effectiveness (SE), time domain finite elements (TDFE), composite materials.

1. Introduction

At present, aircrafts are exposed to variety of external electromagnetic (EM) sources: e.g. TV transmitters, radars, lightning strikes, etc. Such an environment became to be described with an acronym HIRF (High Intensity Radiated Fields). All electronic devices for aircraft industry have to be tested for electromagnetic compatibility (EMC) in high intensity radiated field (HIRF) environment before they can be manufactured with a huge impact in terms of money, time, equipment, space and manpower. In the aim to reduce all the necessary certification cost, it is desirable that part of the measurements will be supported or if possible substituted by numerical simulations.

The Brno University of Technology (BUT) is a member of the collaborative project HIRF Synthetic Environ-

ment (HIRF-SE) supported by the European Commission in the FP7 [1] since 2009. The goal of HIRF-SE, involving 44 partners from 11 European countries, is to provide to the aeronautic industry an EM computational framework to predict the EM environment aboard air vehicles in the presence of a HIRF threat. This tool should support the development and HIRF/EMC certification phase of air vehicles.

Due to various demands of individual devices that need to be modeled, the HIRF-SE Framework embeds plenty of tools including pre- and post-processing tools, frequency domain (FD) full wave solvers and time domain (TD) solvers based on several methods, for example the finite integration technique [2], finite difference method [3], and method of moments [4]. BUT is responsible for the BUTFE tool, the only module based on the Time Domain Finite Element (TDFE) method [5] that will be included in the FW (FrameWork). The Amelet-Hierarchical Data Format (amelet-HDF) format [6] is used as a standard format for the management, storage and exchange of data between the different embedded modules.

The use of the TDFE method for a solution of EMC problems can be found in a few papers only: a brief overview of tested problems can be found in [7]; scattering properties of various shielding structures are computed in [8]; paper [9] describes how the TDFE method can be used to analyze the EM interference generated from individual bars of a bus. This method is also employed for the computation of EM fields generated by lightning return strike in [10].

The paper presents the description of the whole simulation chain inside the HIRF SE platform for the BUTFE module and introduces the computation of the shielding effectiveness (SE) parameter of composite materials using the TDFE method.

The basic fundamentals of the TDFE method are briefly described in Section 2. The TDFE wave equation formulation, time discretization scheme and anisotropic perfectly matched layer (PML) are discussed. Section 3

describes the simulation chain implemented in the HIRF SE FW, discusses the related input and output files, and presents some aspects related to the mesh generation, the choice of the excitation specification and a numerical solution. Section 4 presents an application of the TDFE tool to the computation of the SE of two different composite materials. The numerical results are then validated by the experimental measurements performed by Sapienza University of Rome.

2. Formulation

The behavior of the electromagnetic field in used formulation is described by a wave equation. Depending on simulation settings, the unknown quantity can be either the electric or the magnetic field. The general form of the wave equation for the electric field for a volume Ω (excluding a PML region) limited by the boundary $\partial\Omega$ is:

$$\nabla \times \frac{1}{\boldsymbol{\mu}} \nabla \times \mathbf{E}(\mathbf{r}, t) + \boldsymbol{\sigma} \frac{\partial \mathbf{E}(\mathbf{r}, t)}{\partial t} + \boldsymbol{\varepsilon} \frac{\partial^2 \mathbf{E}(\mathbf{r}, t)}{\partial t^2} = 0 \quad \text{in } \Omega. \quad (1)$$

The symbol \mathbf{E} stands for the electric field vector, σ is the electric conductivity, $\boldsymbol{\varepsilon}$ and $\boldsymbol{\mu}$ are tensors of the permittivity and the permeability, respectively. All three material parameters can be tensors. The boundary conditions can be defined as both Dirichlet and Neumann expressions, which correspond to a perfect electric surface $\partial\Omega_e$ and a perfect magnetic one $\partial\Omega_m$, specifically,

$$\hat{n} \times \mathbf{E} = 0 \quad \text{in } \partial\Omega_e, \quad (2a)$$

$$\hat{n} \times \nabla \times \mathbf{E} = 0 \quad \text{in } \partial\Omega_m \quad (2b)$$

where \hat{n} is the unit vector normal to a particular surface. For the time domain formulation, simple initial conditions are assumed:

$$\mathbf{E}(\mathbf{r}, 0) = 0, \quad \left. \frac{\partial \mathbf{E}(\mathbf{r}, t)}{\partial t} \right|_{t=0} = 0 \quad (3)$$

which corresponds to zero initial energy stored in the computational domain Ω .

The spatial discretization is done in a typical manner, i.e. the weak formulation based on Galerkin procedure is used. Linear vector basis functions $\mathbf{V}_i(\mathbf{r})$ are used also as testing functions. Each basis function corresponds to a particular edge of a tetrahedral mesh.

A weak form formulation [5] can be expressed as

$$\iiint_{\Omega} \left\{ \left[\nabla \times \mathbf{V}_i \right] \cdot \frac{1}{\boldsymbol{\mu}} \left[\nabla \times \mathbf{E}(\mathbf{r}, t) \right] + \boldsymbol{\sigma} \mathbf{V}_i \cdot \frac{\partial \mathbf{E}(\mathbf{r}, t)}{\partial t} + \mathbf{V}_i \cdot \boldsymbol{\varepsilon} \frac{\partial^2 \mathbf{E}(\mathbf{r}, t)}{\partial t^2} \right\} d\Omega = 0 \quad (4)$$

where the electric field is represented as:

$$\mathbf{E}(\mathbf{r}, t) = \sum_{i=1}^N e^i(t) \mathbf{V}_i(\mathbf{r}) . \quad (5)$$

Solving the volume integral in (4) over the whole computational area results in a system of differential equations:

$$\left[S^{\boldsymbol{\mu}^*} \right] e(t) + \left[T^{\boldsymbol{\sigma}} \right] \frac{de(t)}{dt} + \left[T^{\boldsymbol{\varepsilon}} \right] \frac{d^2 e(t)}{dt^2} = 0. \quad (6)$$

Here, the individual entries of the finite element matrices are given by:

$$S_{ij}^M = \int_{\Omega} (\nabla \times \mathbf{V}_i(\mathbf{r})) \cdot \mathbf{M} \cdot (\nabla \times \mathbf{V}_j(\mathbf{r})) d\Omega, \quad (7)$$

$$T_{ij}^P = \int_{\Omega} \mathbf{V}_i(\mathbf{r}) \cdot \mathbf{P} \cdot \mathbf{V}_j(\mathbf{r}) d\Omega, \quad (8)$$

$$\boldsymbol{\mu}^* = \begin{bmatrix} \mu_{xx} & \mu_{xy} & \mu_{xz} \\ \mu_{yx} & \mu_{yy} & \mu_{yz} \\ \mu_{zx} & \mu_{zy} & \mu_{zz} \end{bmatrix}^{-1} \quad \boldsymbol{\varepsilon} = \begin{bmatrix} \varepsilon_{xx} & \varepsilon_{xy} & \varepsilon_{xz} \\ \varepsilon_{yx} & \varepsilon_{yy} & \varepsilon_{yz} \\ \varepsilon_{zx} & \varepsilon_{zy} & \varepsilon_{zz} \end{bmatrix} \quad (9)$$

$$\boldsymbol{\sigma} = \begin{bmatrix} \sigma_{xx} & \sigma_{xy} & \sigma_{xz} \\ \sigma_{yx} & \sigma_{yy} & \sigma_{yz} \\ \sigma_{zx} & \sigma_{zy} & \sigma_{zz} \end{bmatrix}$$

2.1 Time Domain Discretization

Equation (6) is usually solved using a direct integration or a finite difference method [5]. The weighted residual method for the time axis, which is a general approach [11], is used. The time variable t is discretized as $t = n\Delta t$, where Δt denotes the time step and n is a natural number. The unknown coefficients $e(t)$ are approximated in each $2\Delta t$ interval with

$$e(t) = \sum_{i=1}^3 e^i N_i(t) \quad (10)$$

where $N_i(t)$ are second order shape functions.

First, equation (11) is combined with (6) and the result is multiplied by a weighting function and integrated over $2\Delta t$ interval. This approach leads to the following formulas:

$$e(t) = \beta e(n+1) + \left(\frac{1}{2} + \gamma - 2\beta \right) e(n) + \left(\frac{1}{2} - \gamma + \beta \right) e(n-1),$$

$$\frac{de(t)}{dt} = \frac{\gamma}{\Delta t} e(n+1) + \frac{(1-2\gamma)}{\Delta t} e(n-1) - \frac{1-\gamma}{\Delta t} e(n-1), \quad (11)$$

$$\frac{d^2 e(t)}{dt^2} = \frac{1}{\Delta t^2} e(n+1) - \frac{2}{\Delta t^2} e(n) + \frac{1}{\Delta t^2} e(n-1)$$

which yields a scheme equivalent to the Newmark formulation:

$$\begin{aligned}
 & \left\{ \frac{1}{(\Delta t)^2} [T] + \frac{\gamma}{\Delta t} [B] + \beta [S] \right\} \{e\}^{n+1} = \\
 & \left\{ \frac{2}{(\Delta t)^2} [T] - \frac{(1-2\gamma)}{\Delta t} [T] \right. \\
 & \left. + \left(\frac{1}{2} + \gamma - 2\beta \right) [S] \right\} \{e\}^n \\
 & - \left\{ \frac{1}{(\Delta t)^2} [T] - \frac{1-\gamma}{\Delta t} [B] + \left(\frac{1}{2} - \gamma + \beta \right) [S] \right\} \{e\}^{n-1}
 \end{aligned} \quad (12)$$

Here, γ and β are properly chosen coefficients [11].

The scheme (12) is unconditionally stable for $\gamma \geq 1/2$ and $\beta \geq 1/4$ [12]. The recommendation for the optimal time step can be found in [13]:

$$\Delta t = \frac{\Delta x}{c\sqrt{m}} \quad (13)$$

Here, Δx is the minimal length of an edge in the spatial discretization, c is the speed of light and m is the dimension of the problem. For each time step the system consists in a set of linear equations.

2.2 PML Formulation

For solving an open-space problem, we use the most popular algorithm for the termination of a computational domain, namely the perfectly matched layer (PML). PML is an artificial, dispersive and anisotropic medium which, apart from the numerical dispersion, can attenuate incoming waves for any angle of incidence with no reflection at free space simulated by the PML boundary.

The general formulation of wave equation inside the PML region is:

$$\nabla \times \frac{1}{\mu} \left([\Lambda]^{-1} \nabla \times \mathbf{E} \right) - \omega^2 \varepsilon [\Lambda] \mathbf{E} = 0 \quad (14)$$

where $[\Lambda]$ is a diagonal tensor

$$[\Lambda] = \hat{x} \frac{S_y S_z}{S_x} \hat{x} + \hat{y} \frac{S_x S_z}{S_y} \hat{y} + \hat{z} \frac{S_x S_y}{S_z} \hat{z} \quad (15)$$

Here,

$$S_\xi = 1 + \frac{\sigma_\xi}{j\omega\varepsilon_0} \quad \xi = x, y, z \quad (16)$$

Without loss of generality, attenuation in the direction x only can be considered, defined by:

$$\sigma_x = \sigma, \quad \sigma_y = \sigma_z = 0 \quad (17)$$

The same approach [14] can be applied to obtain the system of differential equations:

$$\begin{aligned}
 & [S^I] \frac{1}{\mu} e(t) + \frac{2}{\varepsilon_0 \mu} [S^J] f + \frac{1}{\varepsilon_0^2 \mu} [S^K] g \\
 & + [T^I] \varepsilon \frac{d^2 e(t)}{dt^2} + [T^L] 2\varepsilon_r \frac{de(t)}{dt} \\
 & + [T^R] \frac{\varepsilon_r}{\varepsilon_0} \frac{d^2 e(t)}{dt^2} = 0
 \end{aligned} \quad (18)$$

where

$$f = \int_t edt \quad g = \iint_t edt \quad (19)$$

and the finite element matrices are computed using the same technique as (7) and (8), while M and P are replaced by tensors responsible for a proper PML behavior. The symbol I denotes the identity matrix and the remaining tensors are defined as follows:

$$\begin{aligned}
 J &= \begin{bmatrix} \sigma & 0 & 0 \\ 0 & 0 & 0 \\ 0 & 0 & 0 \end{bmatrix} & K &= \begin{bmatrix} \sigma^2 & 0 & 0 \\ 0 & 0 & 0 \\ 0 & 0 & 0 \end{bmatrix} \\
 L &= \begin{bmatrix} 0 & 0 & 0 \\ 0 & \sigma & 0 \\ 0 & 0 & \sigma \end{bmatrix} & R &= \begin{bmatrix} 0 & 0 & 0 \\ 0 & \sigma^2 & 0 \\ 0 & 0 & \sigma^2 \end{bmatrix}
 \end{aligned} \quad (20)$$

The same approach as in (11) was used for the temporal discretization of (18). Obviously, the unknown quantity is here not only differentiated, but also integrated (compared to (6)). The integration formulas are taken from [14]:

$$f^n = f^{n-1} + \frac{\Delta t}{2} (e^{n-1} + e^n), \quad (21)$$

$$g^n = g^{n-1} + \Delta t e^{n-1} + \frac{\Delta t^2}{4} (e^{n-1} + e^n). \quad (22)$$

Equations (21) and (22) are updated in each time step.

3. Solver

The HIRF SE framework uses various modules, where each module provides at least one of three specific functionalities (pre-processing, post-processing, and analysis). The simulation procedure is usually formed by a chain of modules controlled by the FW environment which allows to set the simulation up, to create an input file, to execute the module and to read the results back from the output file.

Amelet-HDF [6] allows using a single file format within a wide range of numerical EM solvers. The limited wrapper development effort, which was necessary for the integration in the FW of many of the tools, is well compensated by the readability reached through the common format of input and output files.

For each module, several mandatory and optional inputs and outputs have been defined as depicted in Fig. 1. The number in brackets expresses the requested number of objects of a given type. The name of the data type is labeled in italics with the first capital letter (see Fig. 1).

For the TDFE simulation, the chain is formed by a mesh generation, a determination of sources and a main analysis. An optional step is visualization or any kind of post-processing.

The mesh generation is done by a universal GiD module [15] (see Fig. 1), which accepts various optional types of objects. If no object is set as an input, the GiD module allows to define a new geometry and to generate a mesh as an input for a subsequent computational solver/module. The module can produce two types of output data: *Mesh* and *GiD Project*. The simulation saves the resulting mesh into an object *mesh_gid* which is of the type *Mesh*.

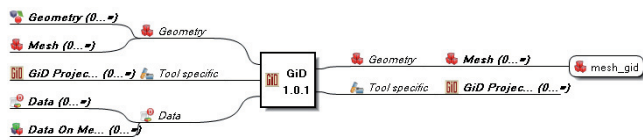


Fig. 1. Mesh generation (GiD).

The excitation is set via a graphical module *BUTFE_EXC* (Fig. 2). The module accepts the previously generated mesh and produces time samples of the excitation. The optimal time step is determined at the start of the program, according to (13) and the provided mesh and the user can modify this value and set the number of the time samples or the desired final time.

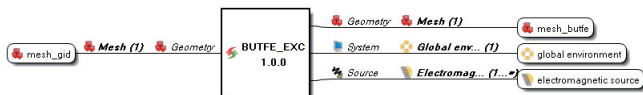


Fig. 2. Sources determination (BUTFE_EXC).

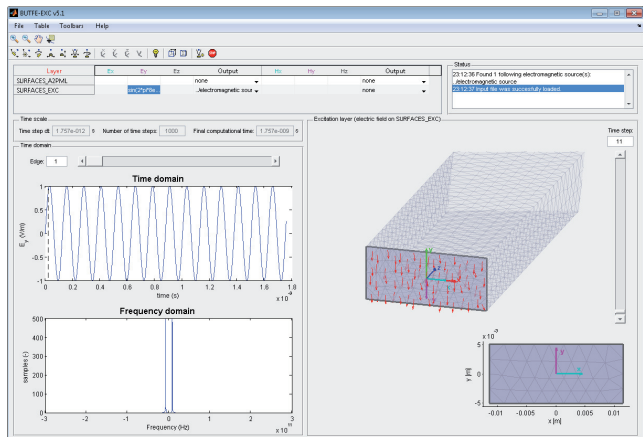


Fig. 3. The BUTFE_EXC module.

A field behavior can be set up in both space and/or time domain (Fig. 3). The module detects available excitation planes of the mesh and converts their coordinates into

a new 2D system. The user can set the space behavior using the transformed coordinates and it is allowed to set the excitation relative to the excitation port rather than the original Cartesian coordinate system.

In order to perform the analysis using a TDFE module *BUTFE* (Fig. 4), data from the *BUTFE_EXC* tool have to be complemented by additional data inputs.

The framework allows defining various types of materials. Vacuum (*Vacuum*) and perfect conductors are predefined, but the user can define his own materials as *Classical material* based on known properties or combine them together in order to form composite materials with more complex geometrical and/or EM properties. The *Link* object has to be created in order to specify relations between any two objects, for example an excitation of a material with a specific part of the mesh.

In order to maintain a reasonable file size, only requested outputs are saved into the output file. The *Output request* object informs the solver on the field to compute and in which point.

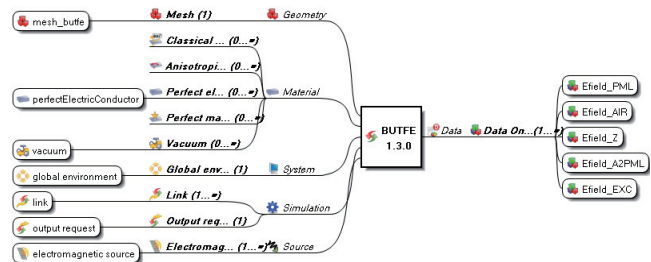


Fig. 4. Numerical analysis of the structure (BUTFE).

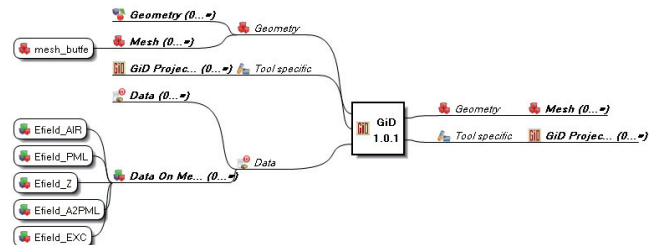


Fig. 5. Visualization (GiD).

The visualization is supposed to be done again by the *GiD* module. The development of some modules linked with the TDFE tool is still in progress, Fig. 5 shows an expected usage only.

In addition, the capability of the FW to handle simulations of cable bundles suggests that the complete simulation chain solving EMC problems can be assembled.

3.1 Description of Input and Output File

Fig. 6 (left) shows a tree structure of the input and output file for the BUTFE (TDFE) module. Each object is described by a path starting with "/". This symbol represents the file root, another "/" symbols indicate one step down in the tree structure (e.g. /mesh/mesh_butfe).

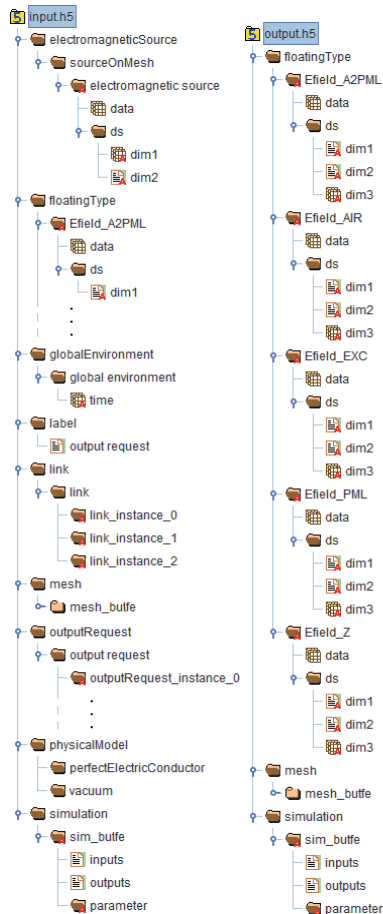


Fig. 6. Input (left) and output (right) file of the BUTFE tool.

User has defined five *output request* instances. Each instance has to contain *subject* (physical quantity to compute), *object* (where to compute that quantity) and *output* (storage for a result). The storage must be a known valid path within the file. In this case, the storage objects are situated in */floatingType* category.

A *subject* of the *output request* instances is stored in */label/output request* dataset. In this case, it contains one string “electricField” only. Thanks to this, the solver knows which type of field to handle with.

Instances of a */link* category link any two objects together. In Fig. 6, the first one connects the electromagnetic source with target layer of the mesh (*/mesh/mesh_butfc/unstructuredmesh/group-/SURFACES_EXC_eg*). The second one links volumetric elements of the layer *.../groupGroup/VOLUMES* with the vacuum material, and the third one connects the boundary layer *.../groupGroup/SURFACES_PEC* with the PEC material.

The path */simulation/sim_butfc/parameter* is determined to contain parameters of the simulation. In this case, it contains three attributes: *maxThreads*, *preconditioner* and *solver*. The first one sets the maximal number of threads to be used for the computation. The default value (zero) sets the number of threads equal to the number of cores available in the system. Remaining attributes pick

a combination from a list of preconditioners / solvers of a mathematical library *Lis* used for the computation [16].

The output file (see Fig. 6, right) has to contain *floatingType*, *mesh* and *simulation* categories to allow the framework reading results back to its database. BUTFE is forming the output file copying the input one and replacing the empty data structures in */floatingType* by the results. It allows saving both the results and all input data for the simulation in a single file. However, the framework reads only the three above mentioned categories.

Results are saved in */floatingType* category. Each particular output contains the dataset *data* (a multidimensional array containing the field values) and group *ds* containing additional three datasets which describe the dimensions of the *data*. Each *.../ds/dim1* contains a path to a particular layer of */mesh/mesh_butfc*, *.../ds/dim2* stores labels of components $\{x, y, z\}$ and *.../ds/dim3* contains a copy of the original time axis stored in */globalEnvironment/global environment/time* of the original input file.

4. Numerical and Experimental Results

In order to validate the TDFE solver, the module is applied to the calculation of the *SE* of two different thin panels of composite materials: a prepreg copper mesh (PCM) and an epoxy resin prepreg carbon fiber (ERPCF).

4.1 Description of Composite Materials

The prepreg copper mesh has a total thickness of 0.12 mm and it is made of copper wires (20 wires per cm) having diameter of 0.05 mm. The wires of the grid form a relative angle of 89 degrees leading to a fairly isotropic structure. The resulting grid is embedded in a non-conductive epoxy resin matrix having electrical permittivity 3.4.

The carbon fiber reinforced composite presents a woven structure with fiber orientation of $0^\circ/90^\circ$ and total thickness of 270 μm . The electrical conductivity of carbon fibers is 220-250 kS/m and their typical diameter is about 7 μm . The permittivity of the non conductive epoxy resin is about 3.4. Fig. 7 shows a microscopic image of the two materials under test.

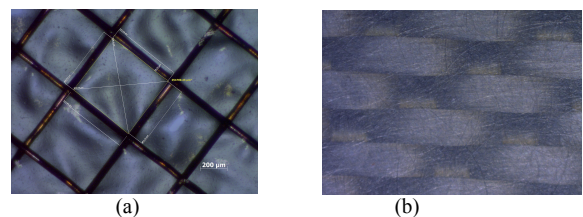


Fig. 7. Microscopic view of the prepreg copper mesh (a) and of the carbon fiber epoxy composite (b) [17] and [18].

The measurement of the *SE* can be used to extract the electrical conductivity for both the materials. An approxi-

mation of such conductivities is depicted in Fig. 8, and it results to be strongly influenced by the trend of the related measurement (see Fig. 12 in Section 4.4).

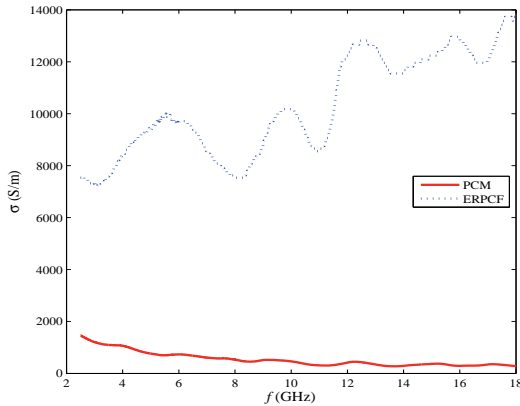


Fig. 8. Conductivity of the PCM and ERPCF homogeneous equivalents [17] and [18].

4.2 Modeling Approach

A general description of the modeling approach is depicted in Fig. 9. A rectangular vacuum-filled waveguide, with aperture laying in the x - y plane and mode propagation along the z -axis, has a cross-section of $60 \text{ mm} \times 4 \text{ mm}$. That corresponds to a cut-off frequency of exactly 2.5 GHz. The total length of the waveguide (z -axis) is 200.27 mm for ERPCF and 200.05 mm for PCM. The waveguide is modeled as a perfect electric conductor (PEC) and it is closed with a PML.

The simulation was run for 3001 steps using a time step $\Delta t = 0.217 \text{ ps}$. The expression of the EM pulse (EXC) orthogonally impinging on the aperture used to excite the waveguide is:

$$EXC = V_{\max} \left\{ \left(\frac{t}{t_r} \right)^{pw} \cdot \exp \left[-pw \left(\frac{t}{t_r} - 1 \right) \right] \right\} \quad (23)$$

with $V_{\max} = 1 \text{ V}$; rise time $t_r = 5\Delta t$ and power $pw = 2$. It has to be noted that the sharp EXC parameters are chosen in order to excite the entire frequency band from 2.5 GHz (lower limit of the rectangular waveguide) up to 18 GHz (upper frequency of the measurements with coaxial setup). The waveguide is assumed to operate in single mode, therefore, the DC component and all frequencies below the cut-off frequency are not considered. The excitation pulse in both time and frequency domain is shown in Fig. 10.

In order to calculate the SE of a composite, a thin (with respect to the wavelength) layer of the material under test is placed at distance d from the aperture. The electric field intensity E of the propagating dominant mode is computed in point P , placed at the center of the waveguide cross-section and at distance p from the aperture, one mm behind the simulated panel.

$$SE = \frac{FFT \{ E^*(P) \}}{FFT \{ E(P) \}} \quad (24)$$

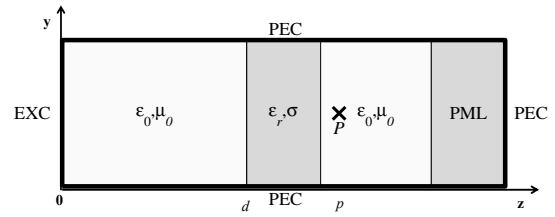


Fig. 9. Description of the modeled problem.

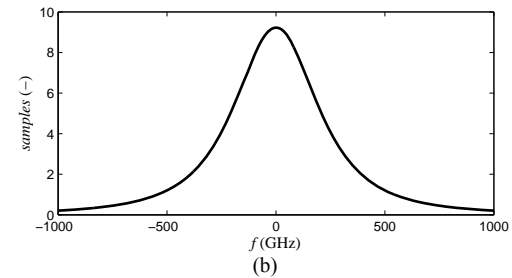
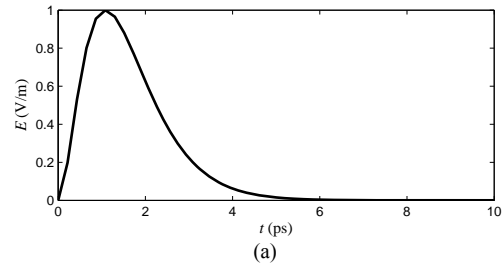


Fig. 10. The excitation pulse in time-domain (a) and frequency-domain (b).

The simulation, using the same mesh and excitation, is run twice: with the empty waveguide and with the composite material placed in. The SE is then computed as the ratio of the Fast Fourier Transform (FFT) of the time samples of the Electric field, with and without the material under test placed in, denoted by $E(P)$ and $E^*(P)$, respectively.

4.3 Experimental Characterization

The simulation results are compared with the measurements of the SE , carried out in the EMCLab of The Department of Astronautical, Electrical and Energy Engineering (DIAEE) at Sapienza University of Rome, [17] and [18]. The experimental tests are performed by applying the coaxial waveguide approach described in the ASTM D4935 [19], [20].

A comparison of the experimental results obtained with a coaxial waveguide with the simulated data from the modeling of a rectangular waveguide is possible because the SE obtained from both methods is representative of the SE of an infinite panel [19], [20].

This method uses a mono-mode (TEM) flanged coaxial sample holder (FCSH) for the shielding effectiveness measurement of flat samples against a plane wave with normal incidence. The test setup consists of a vector network analyzer (VNA), a pair of 50Ω double shielded co-

axial cables, and flanged coaxial sample holders, having different dimensions for each frequency range to be tested as shown in Fig. 11.

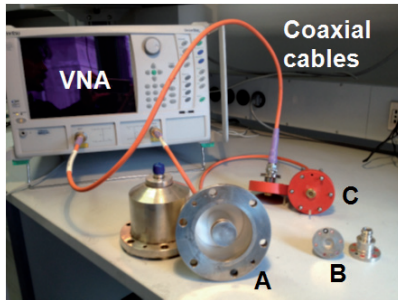


Fig. 11. Picture of the coaxial waveguide measurement setup. The objects named as A, B and C are the different FCSHs used to cover the frequency range from 1 MHz up to 18 GHz [17].

The FCSH is an enlarged coaxial transmission line with an interrupted inner conductor and a flanged outer conductor. The two flanges hold the material sample in the middle of the cell, and are tightly fastened together.

The test procedure consists in measuring the insertion loss (*IL*) according to the [17] standard, defined as the ratio in decibel of the received power, measured with either the reference or the load specimen inserted between the flanges of the FCSH. The expression of *IL* as a function of the measured scattering parameters, S_{21ref} and S_{21load} , of the reference and load specimens, is given by:

$$IL = 20 \log_{10} \left| \frac{S_{21ref}}{S_{21load}} \right|. \quad (25)$$

4.4 Result Comparison and Validation

Fig. 12 shows a comparison between calculated and measured data. It can be noted that the maximum error does not exceed 2 dB in the overlapping frequency range and the trends of corresponding dependencies suggest a very good agreement between measured data and simulated results. The general trend of the PCM shows the ex-

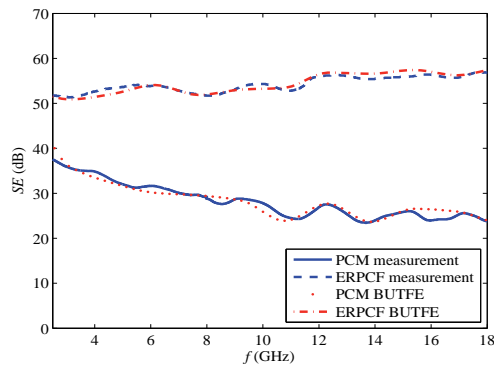


Fig. 12. Comparison of measured and calculated *SE* of the PCM and ERPCF composite materials.

pected so called “grid effect”, a frequency dependant decrease of the *SE* due to the dimension of the grid holes. The same effect is not present for the ERPCF material due to the better coverage provided by the woven texture of the material that leads to a more constant trend of the *SE*.

A further validation analysis is made by using the FSV (Feature Selective Validation) automated GCEM (Grup de Compatibilitat Electromagnètica) tool [21] developed at Universitat Politècnica de Catalunya and widely adopted in the computational electromagnetic field. The FSV method is based on measuring three metrics: Global Difference Measure (*GDM*), Amplitude Difference Measure (*ADM*) and Feature Difference Measure (*FDM*). These three parameters when converted to the natural language description lead to a judgment on the compared sets of data that can run from Excellent to Very Poor. For further information about FSV method please refer to [22].

For the PCM and ERPCF materials, the FSV validations results reported in Fig. 13 (a) and (b), at least 75 % of the compared values lay in Excellent, Very good or Good categories except of the *GDM* measure for the ERPCF material mainly due to the increased mismatch observable between 13 GHz and 15 GHz.

According to total values of FSV parameters obtained by averaging and by applying ad hoc correction factors [21], and reported in Fig. 13 (a) and (b), the comparisons lead to excellent results for both materials and confirm the judgment that an expert eye can give by directly observing the superimposed curves shown in Fig. 12.

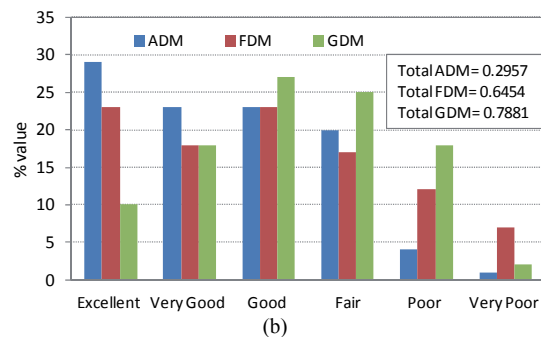
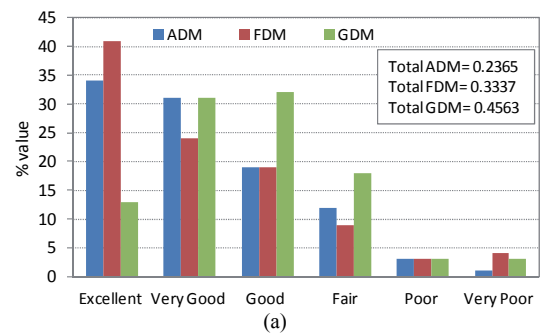


Fig. 13. Summary of point-by-point agreement between measurement and simulation results according to FSV validation: PCM (a) and ERPCF (b) materials.

5. Conclusions

In the paper, an implementation of the time-domain finite-element solver was described, and its integration into the HIRF-SE platform was discussed.

In order to prevent any numerical instability of the solver, an unconditionally stable scheme and an optimal time step were adopted.

The integration of the TDFE solver in the HIRF SE computational framework was presented. The framework was designed to collect and link different kind of modules by providing a user-friendly interface and a common data format.

The TDFE solver was applied to the computation of the SE of two composite materials. The numerical results obtained by BUTFE module were experimentally validated by measurements made by Sapienza University of Rome. The good agreement between measured and simulated data was also confirmed by automatic feature selective algorithms.

Acknowledgements

The work described in this paper has received funding from EC FP7 under grant no. 205294 (the HIRF SE project). Further financing was provided by the Czech Ministry of Education (the grant no. 7R09008).

A support of the project CZ.1.07/2.3.00/20.0007 Wireless Communication Teams financed by the operational program Education for Competitiveness is also gratefully acknowledged.

References

- [1] HIRF SE High Intensity Radiated Field Synthetic Environment [online]. [cit. 2012-01-23]. Available at WWW: <<http://www.HIRF.SE.eu>>.
- [2] WEILAND, T. A numerical method for the solution of the eigenvalue problem of longitudinally homogeneous waveguides. *Electronics and Communication (AEU)*, 1977, vol. 31, p. 308.
- [3] YEE, K. S. Numerical solution of initial boundary value problems involving Maxwell's equations in isotropic media *IEEE Transactions on Antennas and Propagation*, 1966, vol. AP-14, no. 5, p. 302 – 307.
- [4] HARRINGTON, R. F. *Field Computation by Moment Method*. New York: Macmillan, 1968.
- [5] JIN, J. M. *The Finite Element Method in Electromagnetics*. New York: Wiley, 2nd edition, 2002.
- [6] amelet-hdf - Tool Development for Amelet-HDF Specification. - Google Project Hosting [online]. 2009 [cit. 2012-01-23]. Available at WWW: <<http://code.google.com/p/amelet-hdf/>>.
- [7] BRUNS, H. D., SCHUSTER, C., SINGER, H. Numerical electromagnetic field analysis for EMC problems. *IEEE Transactions on Electromagnetic Compatibility*, 2007, vol. 49, no. 2, p. 253 – 262.
- [8] CAORSI, S., CEVINI, G. TDFEM analysis of the scattering properties of shielding structures. In *IEEE International Symposium on Electromagnetic Compatibility*. Istanbul (Turkey), 2003, p. 288 – 291.
- [9] LEI, L., XIANG, C., LEI, Q. Simulation of electromagnetic transients of the bus bar in substation by the time-domain finite-element method. *IEEE Transactions on Electromagnetic Compatibility*, 2009, vol. 51, no. 4, p. 1017 – 1025.
- [10] DE MIRANDA, G. C., RIBEIRO, E. J. Lightning electromagnetic fields computation using time domain finite element method. In *IEEE International Conference on Wireless Communications and Applied Computational*. Honolulu (Hawaii), 2005, p. 301 – 304.
- [11] ZIENKIEWICZ, O.C. A new look at the Newmark, Houbolt and other time stepping formulas. A weighted residual approach. *Earthquake Engineering and Structural Dynamics*, 1977, vol. 5, p. 413 – 418.
- [12] JIAO, D., JIN, J. M. A general approach for the stability analysis of the time-domain finite-element method for electromagnetic simulations. *IEEE Transactions on Antennas and Propagation*, 2002, vol. 50, no. 11, p. 1624 – 1632.
- [13] TAFLOVE, A., HAGNESS, S. C. *Computational Electrodynamics: The Finite-Difference Time-Domain Method*. Boston: Artech House, 2nd edition, 2000.
- [14] TSAI, H. P., WANG, Y., ITOH, T. An unconditionally stable extended (USE) finite-element time-domain solution of active nonlinear microwave circuits using perfectly matched layer. *IEEE Transactions on Microwave Theory and Techniques*, 2002, vol. 50, no. 10, p. 2226 – 2232.
- [15] www.gidhome.com [online]. 2011 [cit. 2012-01-23]. *What's GiD*. Available at WWW: <<http://gid.cimne.upc.es/>>.
- [16] SSI: Scalable Software Infrastructure for Scientific Computing: Lis: a Library of Iterative Solvers for Linear Systems. [online]. 2011 [cit. 2011-12-31]. Available at WWW: <<http://www.ssisc.org/lis/index.en.html>>.
- [17] GRECO, S., TAMBURRANO, A., D'ALOIA, A., MUFFATI, R., SARTO, M. S. Shielding effectiveness properties of carbon-fiber reinforced composite for HIRF applications. In *EMC Europe 2012 Int. Symp. on EMC*. Rome (Italy), 17-21 Sept., 2012.
- [18] BOZZETTI, M., PISU, L., GRECO, S., SARTO, M. S. Shielding performance of an expanded copper foil over a wide frequency range. In *EMC Europe 2011, Int. Symp. on EMC*. York (UK), Sept. 2011.
- [19] SARTO, M. S., TAMBURRANO, A. An innovative test method for the shielding effectiveness measurement of conductive thin films in a wide frequency range. *IEEE Transactions on EMC*, 2006, vol. 48, no. 2, p. 331 – 341.
- [20] *ASTM-D-4935*, Standard method for measuring the electromagnetic shielding effectiveness of planar materials, Sept. 1989.
- [21] *GCEM Validation Tool* [online]. [cit. 2012-10-10]. Available at WWW: <<http://www.upc.edu/web/gcem/>>
- [22] DUFFY, A. P., MARTIN, A. J. M., ORLANDI, A., ANTONINI, G., BENSON, T. M., WOOLFSON, M. S. Feature selective validation (FSV) for validation of computational electromagnetics (CEM). Part I – The FSV Method. *IEEE Transactions on EMC*, 2006, vol. 48, no. 3, p. 449-459.

About Authors ...

Vladimír ŠEDĚNKA (*1983, Ostrava, Czech Republic) graduated at the Faculty of Electrical Engineering and

Communication (FEEC), Brno University of Technology (BUT), in 2009. Since 2009, he has been a post-graduate student at the Dept. of Radio Electronics, BUT.

Jan CIGÁNEK (*1985, Vyškov, Czech Republic) graduated at the Faculty of Electrical Engineering and Communication (FEEC), Brno University of Technology (BUT), in 2010. Since 2010, he has been a post-graduate student at the Dept. of Radio Electronics, BUT.

Petr KADLEC (*1985, Brno, Czech Republic) received his B.S., M.S., and Ph.D. degrees in Electronics and Communications from the Brno University of Technology, Brno, Czech Republic, in 2007, 2009, and 2012, respectively. His current research interests include numerical methods for electro-magnetic field computations and evolutionary algorithms for the optimization of the electro-magnetic components.

Zbyněk RAIDA has graduated at the Brno University of Technology (BUT), Faculty of Electrical Engineering and Communication (FEEC). Since 1993, he has been with the Dept. of Radio Electronics FEEC BUT. In 1996 and 1997, he was with the Laboratoire de Hyperfréquences, Université Catholique de Louvain, Belgium, working on variational methods of numerical analysis of electromagnetic structures. Since 2006, he has been the head of the Dept. of Radio Electronics. Zbyněk Raida has been working together with his students and colleagues on numerical modeling and optimization of electromagnetic structures, exploitation of artificial neural networks for solving electromagnetic compatibility issues, and the design of special antennas. Zbyněk Raida is a member of IEEE Microwave Theory and Techniques Society.

Michal WIKTOR received the M.Sc.E.E. and Ph.D. degrees (with honors) from the Gdansk University of Tech-

nology (GUT), Gdansk, Poland, in 2000 and 2006, respectively. Now he is teaching statistics at Medical University of Gdańsk. His research interests include numerical methods, especially topics related to computer implementation large scale modeling.

Maria Sabrina SARTO (F'10) received the Laurea (summa cum laude) and the Ph.D. degrees in Electrical Engineering from the Sapienza University of Rome, Rome, Italy, in 1992 and 1997, respectively. Since 2005, she has been a Full Professor of Electrotechnics and Electromagnetic Compatibility (EMC) at the Faculty of Engineering, Sapienza University of Rome, where she was also the Director of Research Center on Nanotechnology Applied to Engineering in 2006, the EMC Laboratory of the Department of Electrical Engineering in 1998, and of the Sapienza Nanotechnology and Nanoscience Laboratory in 2011. She has published more than 120 papers in the field of EMC, numerical electromagnetics, advanced materials for EMC. Her current research interests include carbon nanotube interconnects modeling and design, carbon nanotube and graphene-based nanomaterials for EMC, and EMC in aerospace.

Sandra GRECO received the M.Sc. degree in Electronic Engineering and the Ph.D. degree in Electrical Engineering from Sapienza University of Rome, Italy, in 2005 and 2009, respectively. Since 2010 she has been a Postdoctoral Researcher with Sapienza University of Rome. Her research activities are mainly focused on electromagnetic compatibility topics and, in particular, on reverberation chambers and shielding effectiveness theory, measurements and applications. She is a member of the working group IEEE STD 299.1 of the IEEE EMC Society and is actively involved in the FP7 European Project HIRF SE "High Intensity Radiated Field Synthetic Environment".